Bioinspired Batteries: Using Nature-Inspired Materials in Greener and Safer Energy Storage Technologies

Thiago Bertaglia, Luana Cristina Italiano Faria, José Eduardo dos Santos Clarindo, and Frank N. Crespilho

Abstract The widespread use of fossil-based energy sources has led to serious environmental problems, including the greenhouse effect. There is currently an intense search underway to find sustainable ways to generate and store energy and replace fossil fuels. Researchers are actively developing alternatives that are based on natural, biological structures or processes. This worldwide process effort is known as bioinspiration. In this context, quinone and flavin derivatives, which resemble the active molecules in bioenergetic cycles, have been successfully applied in energy-storage devices such as redox flow batteries. These compounds undergo fast reactions, are composed of Earth-abundant elements, and are inexpensive; thus, they can accelerate the advancement of reliable and green energy-storage technology. Furthermore, the need for less invasive and more comfortable approaches to medical care has led to the development of implantable, ingestible, and wearable electronic devices. However, current power sources do not meet the safety and structural requirements of these devices. Bioinspired materials, such as biopolymers, have been extensively explored to produce flexible and smart hydrogels, which can replace liquid electrolytes, and allow the construction of user-friendly, flexible batteries. Hence, recent advancements related to the use of bioinspired materials in battery design and fabrication are discussed in this chapter.

1 Introduction

There is currently an urgent need for novel energy-storage devices (ESDs) in a diverse range of technologies. ESDs are required at every size scale, both large and small. At the larger end of the scale, new approaches are needed to address concerns with intermittent renewable energy sources that include solar and wind power. Intermittency can lead to energy shortages that cause human and economic losses [1, 2]. At the smaller end of the scale, the next wave of healthcare-related

T. Bertaglia · L. C. Italiano Faria · J. E. dos Santos Clarindo · F. N. Crespilho (✉)
University of São Paulo, São Carlos Institute of Chemistry, Avenida trabalhador São-carlense, 400, São Carlos, São Paulo, Brazil
e-mail: frankcrespilho@usp.br

electronics will obtain physiological data in ways that are minimally invasive and convenient to the user [3]. These aims cannot be achieved using the current rigid power sources, which makes it imperative to develop wearable and flexible ESDs [4, 5]. Thus, researchers are devising strategies to overcome these challenges as well as promote sustainable development on a global basis.

Over billions of years, nature has developed complex processes and hierarchical materials to address the needs of living organisms [6]. Bioenergetic transformations reach their pinnacle in cellular respiration and photosynthesis pathways. These complex pathways use organic molecules, including quinones and flavins, to capture and store energy from the oxidation of small organic molecules and sunlight, respectively [7–9]. Both of these magnificent processes provide a rich treasure-trove for investigators in energy-storage-related fields seeking ideas and alternatives for designing new technologies. At the structural level, nature has countless examples of biopolymers, such as gelatin, chitin, and alginate, which are interesting alternatives for the production of biocompatible, biodegradable, and cheap hydrogels [10]. These soft materials possess flexibility, can achieve high conductivity, and are less prone to leakage, thus meeting the safety and structural requirements of the latest electronic devices [4, 11]. This chapter will cover the recent bioinspired approaches used in the energy-research field. The application of bioinspired molecules in redox flow batteries is reviewed. Finally, the use of natural hydrogels to produce a new generation of aqueous batteries is also discussed.

2   Redox Flow Battery

Redox flow batteries (RFBs) are electrochemical systems capable of converting electrical energy into chemical energy that is stored in tanks outside the electrochemical cell. The full assembly is composed of an electrochemical cell, storage tanks, and pumps to circulate the electrolyte. Figure 1a shows the components of the electrochemical cell, which include endplates, current collectors, graphite flow fields, gaskets, electrodes, and a membrane. Cell function is initiated by pumping the electrolyte from the storage tanks, which brings the active compounds into contact with the electrodes surfaces, where the electrochemical reactions occur (Fig. 1b). The gasket prevents electrolyte leakage and the membrane prevents electrolyte mixing [12].

RFB systems may be classified according to the nature of the active compound, solvent, and physical state of the electrodes. The active compounds employed can be inorganic and organic, for example, in vanadium- and quinone-based RFBs, respectively. The solvent used to carry the active compounds to the electrode surface is either aqueous or non-aqueous, and both types of solvent can be applied in organic and inorganic RFBs. The active compounds can be in one or two physical states: dissolved in the electrolyte or loaded on the electrode surface. In a hybrid flow battery (HFB), one of the compounds is on the electrode [13, 14]. Figures 1b, c show the two different approaches.
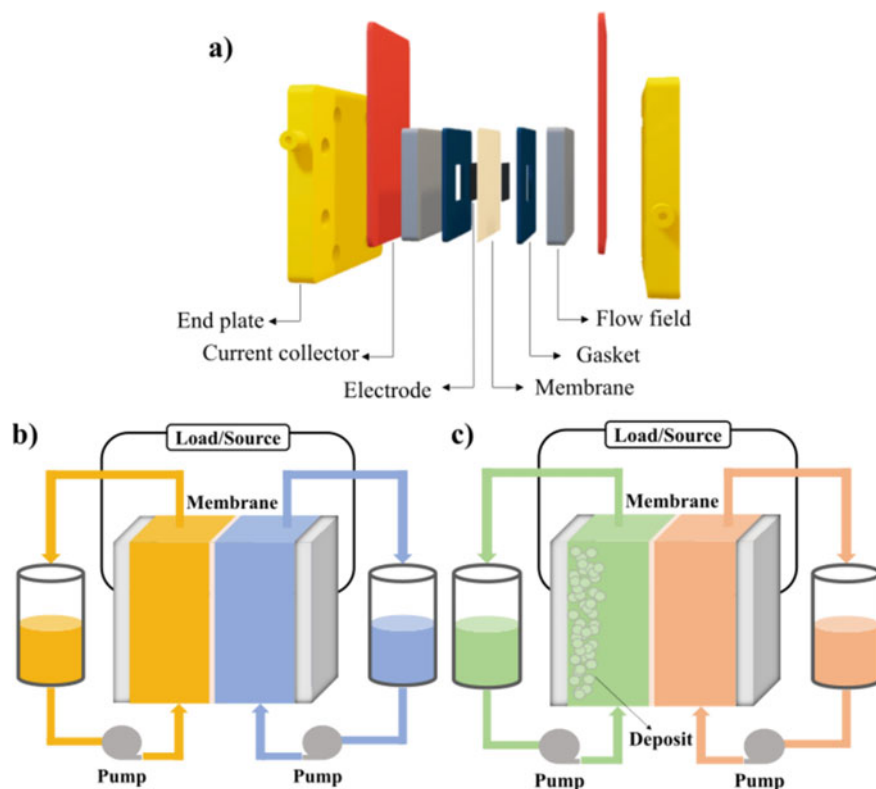
Fig. 1 a Illustration of RFB hardware with cell stack components. **b** Schematic representation of a redox flow battery. **c** Schematic representation of a hybrid flow battery. A material is electrodeposited on the electrode when charging the battery

RFBs have a flexible modular design, moderate maintenance costs, excellent scalability, and a long life cycle [15], which makes them a promising solution for the intermittency issues of natural energy sources, such as wind, solar, and tides. Vanadium RFBs (VRFBs) were the first to be explored commercially [16]. This technology uses active vanadium compounds in highly acidic electrolytes (3–4 mol L^{-1} H$_2$SO$_4$) that are present on both sides of the battery, with vanadium in all four redox states [17]. Despite their high reversibility and stability, vanadium salts have a high cost, are toxic, can precipitate at both high and low temperatures [18], and have reduced solubility at high acid concentrations [19]. These drawbacks hinder the widespread implementation of the VRFB technology.

Some alternatives to vanadium compounds have been extensively studied. Aqueous organic RFBs (AORFBs) use soluble organic compounds that undergo reversible electrochemical reactions. This type of battery has received much attention during the last two decades. Organic molecules are composed of Earth-abundant

elements, may be safe to use, have a potentially low cost [20–23], and can be conveniently changed by inserting donor and withdrawn groups [24, 25]. Some examples of organic/organometallic compounds that have been employed are quinone derivatives [26–33], viologen radicals [34–38], nitroxide radicals (4-HO-TEMPO) [34, 38–40], flavin derivatives [41, 42], and ferrocene derivatives [36, 37]. Among these compounds, quinones and flavins play a key role in biological energy-conversion systems and are promising active compounds for AORFB production. The following section discusses the latest advancements in quinone- and flavin-based AORFBs.

2.1   Quinone-Based Aqueous Organic Redox Flow Battery

Quinones are one of the most important and well-studied examples of organic redox couples. They are widespread in nature and are part of the electron transport chain involved in cellular respiration and photosynthesis, for example, ubiquinone and plastoquinone, respectively [7, 43]. Additionally, numerous applications for this type of molecule have been found, including tinctures, and as oxidizing and reducing agents in industrial and laboratory-scale chemical syntheses [43]. Quinones are classified according to the number of aromatic rings (Fig. 2): benzoquinone with one ring, naphthoquinone with two rings, and anthraquinone and phenanthrenequinone with three rings. The structural diversity of quinones allows for electrochemical adaptation, enabling the construction of sustainable ESDs [44].

Quinone molecules have been employed in RFB development since 2009, when Xu et al. [45] reported an HFB using a chloranil-carbon black composite as the cathode and electrodeposited cadmium as the anode. About a year later, the same research group reported an HFB using 1,2-benzoquinone-3,5-disulfonic acid (BQDS) as the positive active compound and a lead plate as the negative active material [46]. These seminal works presented the possibility of building flow batteries using organic molecules, both on the electrode surface and in solution, and created this new research field. Currently, there is a large demand for highly soluble quinone derivatives that can enhance the battery volumetric capacity and power density [47].

The stability of BQDS in acidic media has been extensively studied by Yang et al. [27]. To this end, the authors developed an all-organic aqueous RFB using BQDS as the cathode and anthraquinone-2-sulfonic acid (AQS) as the anode, with both dissolved in 1 mol L^{-1} H_2SO_4 electrolyte. They found that due to the fact that BQDS has sulfonic acid groups in its structure, there is stabilization by intramolecular hydrogen bonding, because benzoquinone has a solubility of 0.1 mol L^{-1}, while BQDS, which has two sulfonic groups, has a solubility of 1.7 mol L^{-1}. This cell showed a capacity-retention rate of 90% at 10 mA cm^{-2} for 12 cycles. In 2016, new studies were conducted using BQDS and 9,10-anthraquinone-2,7-disulfonic acid (AQDS) [48]. The authors employed the NMR technique and proved that BQDS exhibits several chemical and electrochemical transformations during battery cycling and undergoes a Michael reaction. This study demonstrates the necessity of AQDS
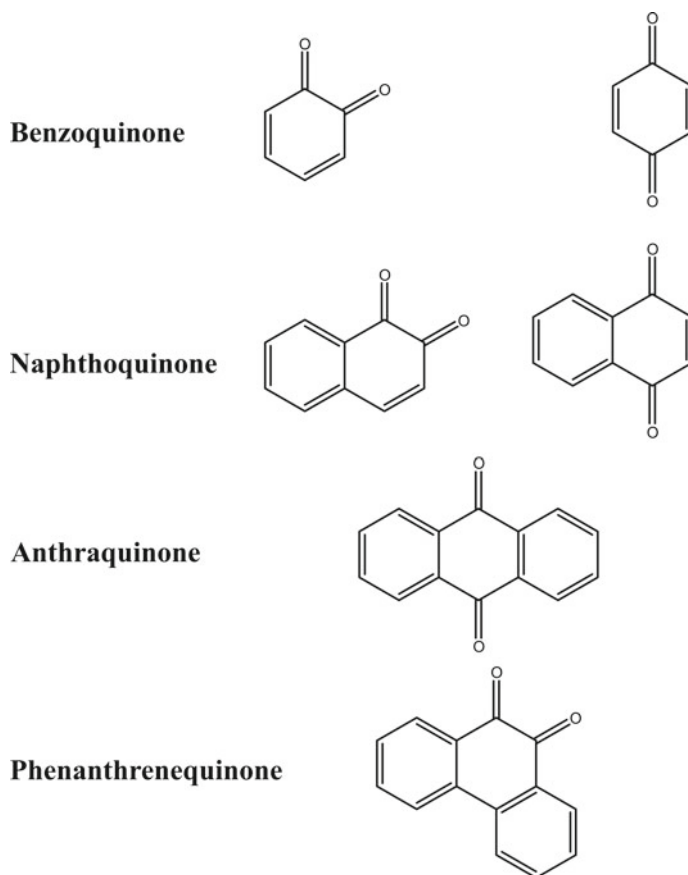
Fig. 2 Different types of quinones and their structures

concentrations that are three times higher than that of BQDS. This battery achieved a coulombic efficiency (CE) of 100% over the course of 100 cycles.

Huskinson et al. [20] reported a high power-density battery that couples the AQDS and Br$_2$/HBr redox pair under acidic conditions. Cycling studies at 0.2 A cm^{-2} at 50% state of charge (SOC) resulted in reproducible cycles with a current efficiency close to 95%. At a current density of 0.5 A cm^{-2} and a cut-off voltage of 0 V and 1.5 V, the discharge capacity retention was 99%. Furthermore, the polarization and power curves for SOCs ranging from 10 to 90% display an increase in the open-circuit voltage (OCV) and peak power densities from 0.69 V to 0.92 V, and 0.246 W cm^{-2} to 0.600 W cm^{-2}, respectively.

Lin et al. [23] reported an adaptation to an alkaline battery, where bromine was replaced with the non-toxic K$_4$[Fe(CN)$_6$] complex, and anthraquinone was functionalized with hydroxyl groups. This approach expanded the battery voltage. The cell was assembled by coupling 2,6-dihydroxyanthraquinone (2,6-DHAQ) and

$K_4[Fe(CN)_6]$ in the negative and positive chambers, respectively. The Pourbaix diagram depicted that 2,6-DHAQ undergoes two-proton two-electron reaction until it reaches pH 12. Above this pH, there is no potential changing since the reduction species were produced in their fully deprotonated form. The charged battery showed an OCV of 1.2 V at 50% SOC and a peak galvanic power density exceeding 0.4 W cm^{-2} in a power curve. Galvanostatic charge/discharge cycles were conducted with a current density of 0.1 A cm^{-2} for 100 cycles, resulting in current and energy efficiencies of 99% and 84%, respectively. In addition, the battery exhibited a capacity fade of 0.1% per cycle over 100 cycles.

Because of the increasing interest in quinones for RFB applications, a theoretical study covering approximately 50 anthraquinone derivatives was carried out by Bachman et al. [25]. They performed density functional theory calculations to determine electrochemical properties, including the substitution effect for electron acceptor and withdrawing groups, redox windows, and free solvation energy. The study showed that substitution by electron donor groups improves the anthraquinone reduction window, with adequate oxidative stability; this is useful for designing new active redox compounds.

Recently, Lee et al. [26] reported an alkaline RFB that uses a mixture of naphthoquinones. The negolyte comprised of a mixture of a sodium salt of 1,2-naphthoquinone-4-sulfonic acid (NQ-S) and 2-hydroxy-1,4-naphthoquinone (Lawsone). $K_3[Fe(CN)_6]$, was used as the posolyte. This mixture of naphthoquinones showed a higher solubility in KOH (1.26 mol L^{-1} in 1 mol L^{-1} KOH) than in individual studies of 0.42 mol L^{-1} and 0.83 mol L^{-1} in 1 mol L^{-1} KOH for Lawsone and NQ-S, respectively. This increase is because NQ-S releases the hydrophilic sulfite ($-SO_3{}^{2-}$) group during the transformation, and it can form polar-polar interactions with organic species and KOH electrolyte. This battery, with 0.6 mol L^{-1} NQ-SO (mixture of NQ-S and Lawsone) and 0.4 mol L^{-1} $K_4[Fe(CN)_6]$ has a voltage of 1.01 V, with a discharge capacity of 22 Ah L^{-1} at 70% SOC. When the NQ-SO concentration was increased to 1.2 mol L^{-1}, the discharge capacity increased to 40.3 Ah L^{-1} at 83% SOC.

Two new synthetic anthraquinones based on 9,10-dihydroanthracene were developed for use on the negative side of an RFB. 3,3′-(9,10-anthraquinone-diyl)bis(3-methylbutanoic acid) (DPivOHAQ) and 4,4′-(9,10-anthraquinone-diyl)dibutanoic acid (DBAQ) were each paired with $K_4[Fe(CN)_6]$ at pH 12 [49]. DBAQ had a solubility of 1 mol L^{-1}, and DPivOHAQ had a solubility of 0.74 mol L^{-1}. The full cell exhibited a capacity fade rate of 0.0084% per day with DBAQ, and 0.014% per day with DPivOHAQ (Fig. 3a). Furthermore, when DPivOHAQ was exposed to air, and the pH was increased to 14, the cell had a capacity fade rate of 0.0018% per day. This equates to a record low-capacity fade rate of 0.66% per year (Fig. 3a). This change in capacity fade rate with increasing pH was attributed to anthrone formation because an increase in the hydroxide concentration can suppress the formation of anthrone, beyond its exposure to air, and can convert back to anthraquinone. Figures 3b, c show the charge–discharge voltage curves with 0.5 mol L^{-1} DPivOHAQ-$K_4[Fe(CN)_6]$, and indicate a steep profile followed by a short horizontal segment. It was possible to
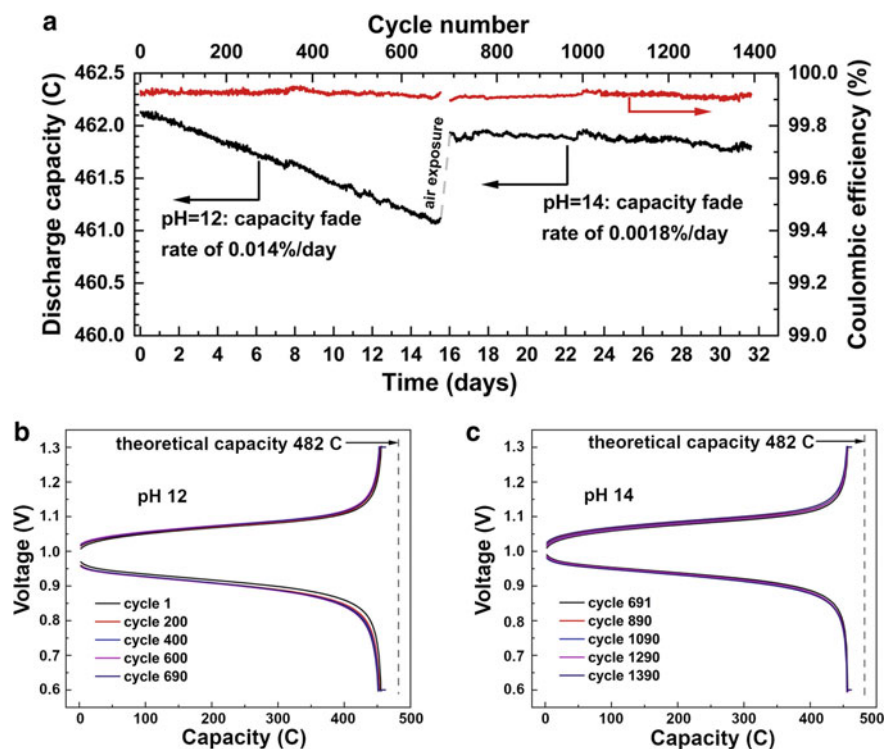
Fig. 3 Cycling performance of DPivOHAQ at pH 12 and 14. **a** CE and discharge capacity versus time and cycle number for a full cell. After approximately 16 days of cycling, DPivOHAQ was exposed to air and the pH of all electrolytes was adjusted to 14 before cycling for another 16 days. **b** Charge–discharge voltage profile of DPivOHAQ from selected cycles at pH 12 in Fig. 3a. **c** Charge–discharge voltage profile of DPivOHAQ from selected cycles at pH 14 in Fig. 3a. Reprinted from Chem, v.6, Wu, M. et al., Extremely Stable Anthraquinone Negolytes Synthesized from Common Precursors, p. 1432–1442, Copyright (2021), with permission from Elsevier

conclude that the electrolyte has approximately 4.5% inactive material, because the horizontal segment ends at 95.5% of the theoretical capacity.

In situ electrosynthesis was conducted by oxidizing a water-soluble anthracene in anthraquinone without the use of oxidants or catalysts, producing the anolyte DPivOHAQ and $K_3[Fe(CN)_6]$ as a catholyte [50]. This is a promising approach because it does not use hazardous materials or require further product purification, which lowers the cost and environmental impact. A charge–discharge test for a single cycle resulted in an OCV equal to 1.0 V, and a capacity of 84 C. Then, 2271 cycles were performed over 33.2 days, with a fade rate of 0.014% per day and CE of 99.53%. The low fade rate was due to the chemical stability of the molecular structure. Therefore, the two branched methyl groups on the anthraquinone core increased the stability of the solubilizing chain. Furthermore, there is a C–C covalent bonding

between the anthraquinone core and the functionalizing chains that is more robust at a high pH and elevated temperature.

The influence of the structure of carbon-based electrodes on the electrochemical kinetics of quinones was studied by Sedenho et al. [51]. Glassy carbon (GC), highly ordered pyrolytic graphite (HOPG), and high-edge-density graphite (HEDGE) were chosen as electrode materials because of the different degrees of defects in their structures. Among the three materials, HEDGE presented the highest degree of edge defects, followed by GC, which presented fewer defects, and HOPG, which had almost no defects. Furthermore, the authors employed four quinone derivatives, namely frog quinone (FQ), crab quinone (CQ), BQDS, and Alizarin Red S (ARS), which can be used as a cathode, or in symmetric batteries.

Figure 4 shows the electrochemical behavior of the four quinones studied. All quinones displayed reversible cyclic voltammograms (CV) using the HEDGE electrode, which does not occur with the HOPG and GC electrodes. Furthermore, the CV for HEDGE suggests an electrochemical process that was controlled by adsorbed species on the electrode surface. For instance, the CV of CQ using the HOPG electrode shows a broad oxidation peak and a major reduction peak, with a peak separation (ΔE_p) of 570 mV, which means there is a quasi-reversible reaction. With the GC electrode, the CV for CQ shows a broad oxidation and reduction peak, with a smaller ΔE_p (330 mV). Conversely, the CV of CQ on the HEDGE electrode has well-defined oxidation and reduction peaks, with an ΔE_p of 30 mV, which indicates a reversible reaction controlled by adsorbed species on the electrode surface. Additionally, the CV for ARS shows remarkable differences. GC and HOPG electrodes exhibit similar electrochemical behavior, with a quasi-reversible redox pair at lower potential (approximately −0.20 V) attributed to the 9,10-quinone moiety. Also, the reactions of the 3,4-dihydroxyl groups occur only during the oxidation wave and are considered irreversible. In contrast, the CV of ARS using the HEDGE electrode suggests reversible electrochemical processes at both low and high potentials, with ΔE_p values of 21 and 11 mV, respectively. These results demonstrate the effects of the electrode structure on the electrochemical behavior of the quinones [51].

To understand the electrochemical behavior of HEDGE, its structure was evaluated using spectroscopic measurements and theoretical calculation. Raman measurements showed that HEDGE presents a highly-defective structure, because the I_D/I_G ratio of this electrode was 0.45, which is much higher than the I_D/I_G ratio for HOPG (0.09). Additionally, X-ray photoelectron spectroscopy indicated the presence of oxygenated groups on the HEDGE surface in the form of hydroxyl, ether, and carbonyl functional groups. This structure was further simulated through molecular dynamics, and the role of the defects in the quinone-electrode surface interaction was evaluated. The results show that quinone molecules interact with HEDGE via van der Waals forces (Fig. 5), mainly between the carbon atoms of the carbonyl moieties and the heteroatoms present in the chemical structures of the quinones, such as nitrogen (FQ and CQ) and sulfur (ARS and BQDS). Therefore, the authors concluded that the highly-defective structure of HEDGE and the functional groups present on its surface stabilize the quinone derivatives, which favors their electrochemical kinetics [51].
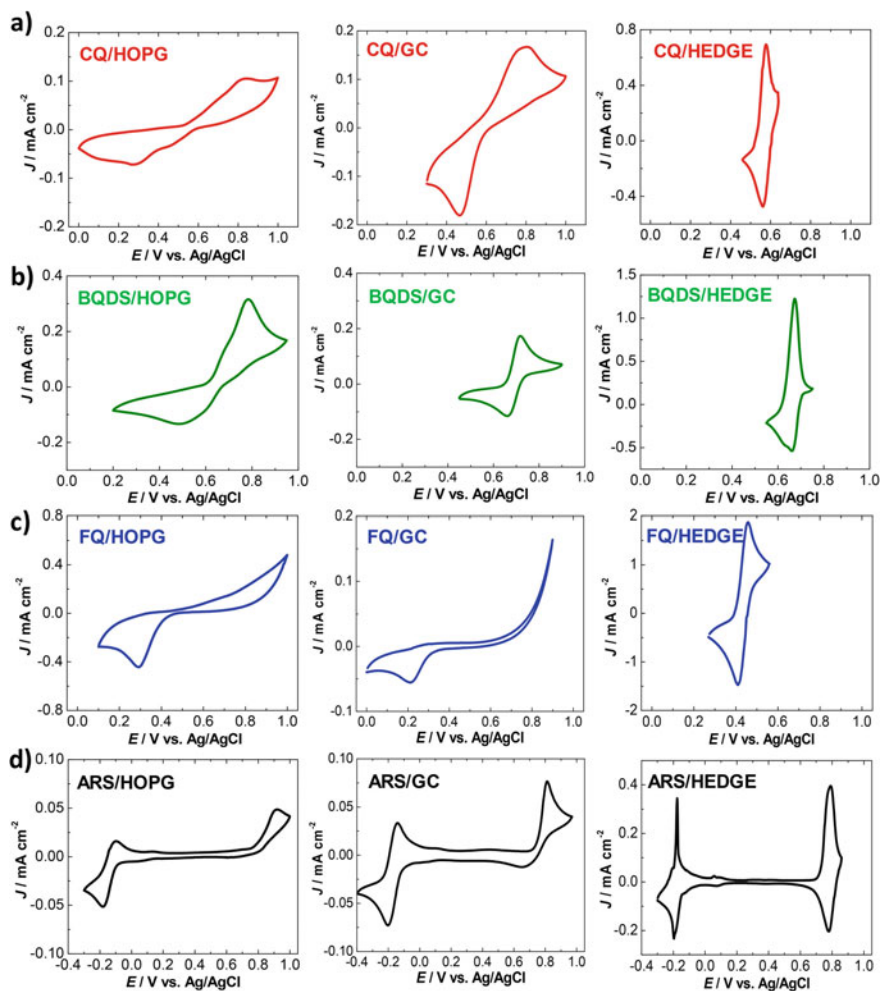
Fig. 4 Cyclic voltammograms for **a** CQ, **b** BQDS, **c** FQ, and **d** ARS at acid media using GC, HOPG, and HEDGE electrodes. Reprinted (adapted) with permission from Ref. [51]. Copyright 2021 American Chemical Society

2.2 Flavin-Based Redox Flow Battery

Another interesting class of organic molecules used in bioinspired batteries is flavins (Fig. 6), which act as a cofactor in several enzyme-catalyzed biological reactions [9, 52]. Flavins are heterocyclic compounds that can undergo a redox reaction by transferring one or two electrons and reacting with oxygen, which includes the formation of adducts [53, 54]. Riboflavin, which is composed of an isoalloxazine unit, is vitamin B$_2$ [52]. Furthermore, in addition to the basic structure of riboflavin, flavin
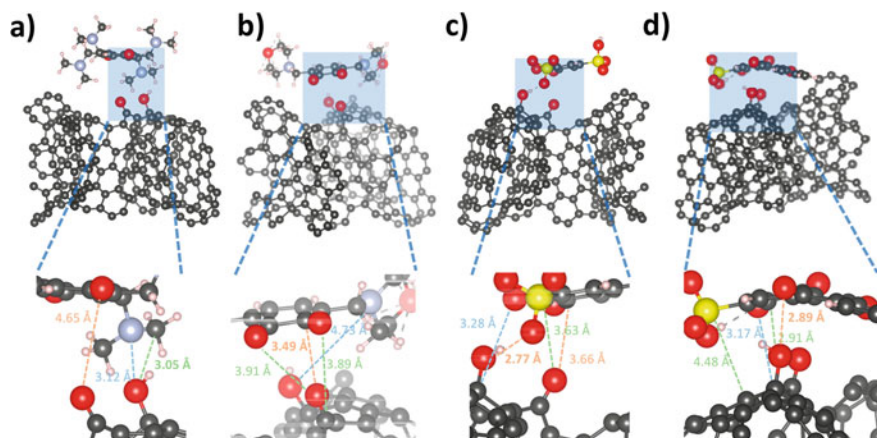
Fig. 5 Molecular dynamics simulations of the quinone-HEDGE interaction for **a** FQ, **b** CQ, **c** BQDS, and **d** ARS. The gray, yellow, red, and blue spheres denote carbon, hydrogen, sulfur, and oxygen atoms, respectively. Reprinted (adapted) with permission from Ref [51]. Copyright 2021 American Chemical Society
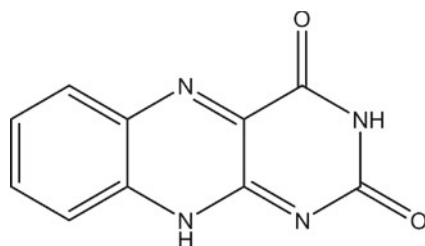

Fig. 6 Chemical structure of flavin

mononucleotide (FMN) and flavin adenine dinucleotide are also formed by the planar isoalloxazine ring [42]. This type of organic compound is versatile because of the various redox states that the flavin ring can adopt [52], and it can be dissolved in water, fat, blood, as well as in biological systems [42]; thus, flavins are promising materials for bioinspired-RFB development.

Orita et al. [42] developed a bioinspired aqueous RFB using flavin mononucleotide sodium salt (FMN-Na) as the negative electrolyte and $K_4[Fe(CN)_6]$ as the positive electrolyte. Although FMN-Na has the highest hydro solubility compared to other flavins, nicotinamide was used as a hydrotropic agent in its electrolyte to further increase its solubility. This high solubility is due to FMN-Na having a higher polarity in alkaline solutions than in acidic or neutral solutions. The polarity is caused by the large negative charge (FMN^{3-}), resulting in the most stable solvated state by water. The half-cell study showed that FMN-Na responds better in alkaline media, since the CV displayed higher current densities and lower peak separations.

The electrochemistry of the battery was tested at both low and high concentrations. First, the RFB was assembled using 0.06 mol L^{-1} FMN-Na and 0.1 mol L^{-1} K$_4$[Fe(CN)$_6$] in 1 mol L^{-1} KOH, which gives a theoretical capacity of 1.34 Ah L^{-1}. The charge–discharge curves were obtained in galvanostatic mode using current densities of 5, 10, and 20 mA cm^{-2}. Figure 7a shows the obtained results. The initial discharge capacity at 10 mA cm^{-2} was 1.31 Ah L^{-1}, which is close to the theoretical value. Figure 7b shows the 1st, 100th, and 200th cycles of the galvanostatic charge–discharge measurement at 10 mA cm^{-2}. Over 200 cycles, stable discharge capacities and an increase in CE were observed (Fig. 7c). However, there are two
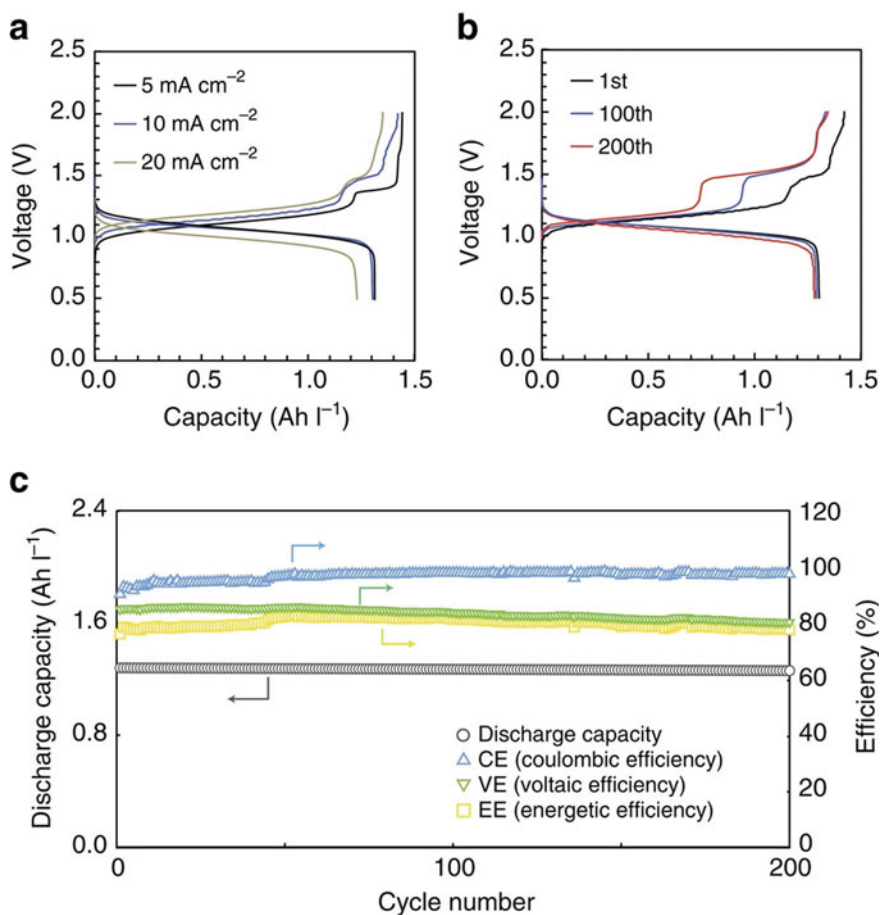

Fig. 7 Electrochemical performance of an RFB assembled with 0.1 mol L^{-1} K$_4$[Fe(CN)$_6$] and 0.06 mol L^{-1} FMN-Na in 1 mol L^{-1} KOH. **a** Charge–discharge curves at 5, 10, and 20 mA cm^{-2}. **b** Charge–discharge at 1st, 100th, and 200th cycles at 10 mA cm^{-2}. **c** Discharge capacity and coulombic, voltaic, and energetic efficiencies for the assembled K$_4$[Fe(CN)$_6$]/FMN-Na RFB at 10 mA cm^{-2}. Reproduced with permission from Ref. [42] with the copyright of Springer Nature

plateaus, at 1.15 and 1.50 V, in the load curve, which suggests a reduction of the FMN-Na monomer and dimer.

Then, the concentration of the electrolytes was increased, and a new RFB was studied, using 0.4 mol L^{-1} $K_4[Fe(CN)_6]$ in 1 mol L^{-1} KOH and 0.24 mol L^{-1} FMN-Na and 1 mol L^{-1} nicotinamide in 1 mol L^{-1} KOH. The charge–discharge profile (Fig. 8a) was analyzed at current densities of 10–80 mA cm^{-2}. The two charge plateaus previously observed were only seen at 10 and 25 mA cm^{-2}. Thus, lower charge capacities were observed at higher current densities. The initial capacity obtained at 25 mA cm^{-2} was 5.03 Ah L^{-1}, which is close to the theoretical value for the RFB (5.36 Ah L^{-1}). Charge–discharge curves, cycling discharge capacities, and efficiencies were obtained over 200 cycles, lasting 76 h at current densities of 50 and 80 mA cm^{-2} (Fig. 8b, c). Figure 8c shows that 99% of the discharge capacity was retained after 100 cycles, and the CE was greater than 99% at 80 mA cm^{-2}. Figure 8d shows the power curve, indicating a peak power density equal to 0.16 W cm^{-2} at 0.3 A cm^{-2}, which is greater than that of the VRFB (0.12 W cm^{-2} at 0.15 A cm^{-2}).

Orita et al. [42] proposed that resonance structures in the reduced state allow for stable redox cycle performance. They also project new studies with other positive electrolytes that have even greater solubility in water. They concluded that FMN-Na is a promising active material for RFBs, in part because it is highly abundant, and not harmful to the environment.

Another study using flavin derivatives was published by Lin et al. [41]. It reported alloxazine-based, meaning a tautomer of the isoalloxazine structure of vitamin B_2, active material on the negative side and a mixture of $K_4[Fe(CN)_6]$/$K_3[Fe(CN)_6]$ on the positive side. However, because alloxazine has low solubility, the alloxazine core was functionalized with an alkaline-soluble carboxylic acid group by reacting o-phenylenediamine-4-carboxylic acid with alloxan to produce an isomeric mixture of alloxazine 7/8-carboxylic acid (ACA). Then, an aqueous RFB was assembled using 0.5 mol L^{-1} ACA as a negative electrolyte and 0.4 mol L^{-1} $K_4[Fe(CN)_6]$ + 40 mmol L^{-1} $K_3[Fe(CN)_6]$ as a positive electrolyte; both electrolytes were adjusted to pH 14 in KOH. This cell had an OCV of 1.2 V. Looking at the polarization curve, it is possible to observe a peak power density of 0.35 W cm^{-2} at a current density of 0.58 A cm^{-2}. Additionally, after 400 cycles, a current efficiency of 99.7% at 0.1 A cm^{-2} was achieved; however, the energy efficiency is only 63% (presumably due to an increase in system resistance), while the capacity-retention rate is greater than 91%. Therefore, considering new systems, they simulated, through theoretical modeling, two other molecules, also derived from alloxazine, which indicates an additional increase of almost 10% in the battery voltage. Thus, these bioinspired molecules offer a promising avenue for the development of AORFBs.
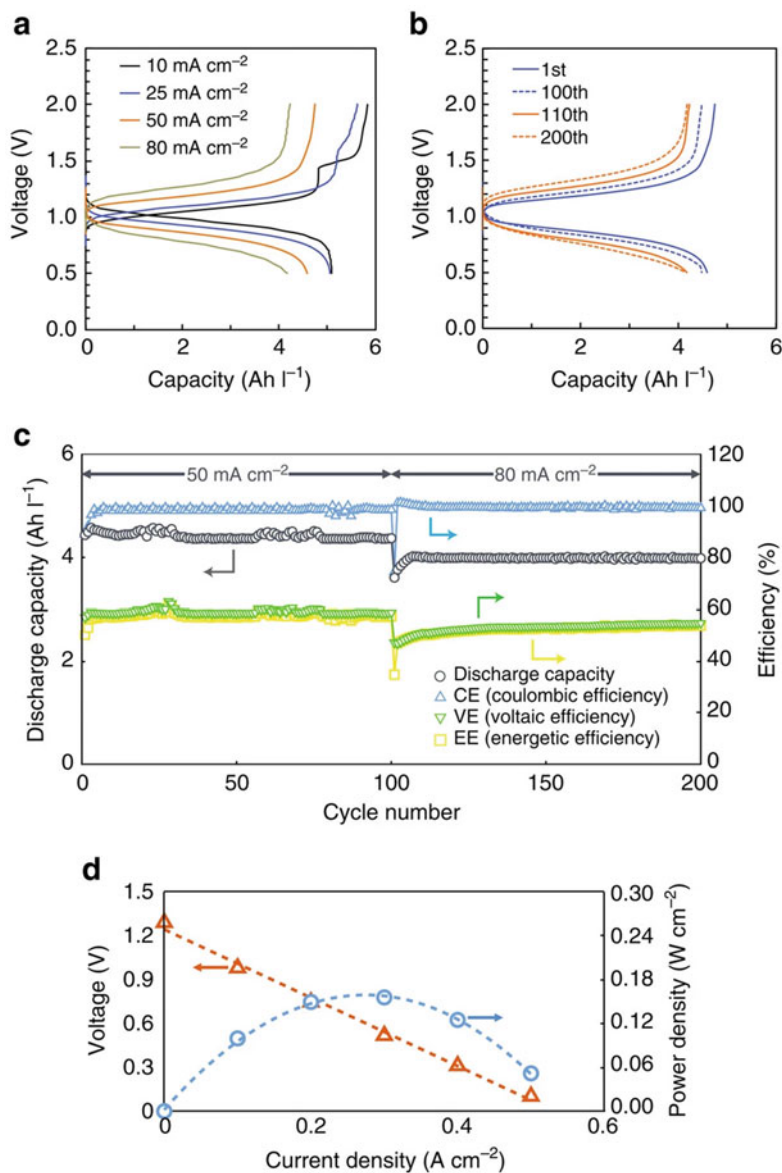
Fig. 8 Electrochemical performance of an RFB assembled with 0.4 mol L^{-1} K$_4$[Fe(CN)$_6$] and 0.24 mol L^{-1} FMN-Na in 1 mol L^{-1} KOH and 1 mol L^{-1} NA. **a** Charge–discharge curves at 10, 25, 50, and 80 mA cm^{-2}. **b** Charge–discharge curves at 1st and 100th cycles at 50 mA cm^{-2}, and 110th and 200th cycles at 80 mA cm^{-2}. **c** Discharge capacity and coulombic, voltaic, and energetic efficiencies over 200 cycles. **d** Cell voltage vs current density vs power density for a high concentration of K$_4$[Fe(CN)$_6$] / FMN-Na RFB. Reproduced with permission from Ref. [42] with the copyright of SpringerNature

3   Bioinspired Electrolytes: Using Biopolymers to Produce Greener and Safer Electrolytes

Wearable, ingestible, and implantable devices are currently at the cutting-edge of research and are applicable to many areas of technology, including healthcare [5, 55]. Although these technologies present many advantages, there is a lack of reliable and safe energy-storage components that meet the requirements of these devices [5]. Lithium-based batteries and silver-silver oxide are currently most often used as power sources in these devices, but they present concerns that include gastric juice pH enhancement [55, 56], toxic electrolyte leakage [57], and skin burning [58]. Thus, the development of reliable and safe batteries is an important step in the further development of these technologies.

Hydrogels are defined as 3D cross-linked networks capable of absorbing water without dissolving, and exhibit viscoelastic rheological behavior [59, 60]. Figure 9a depicts the basic structure of a hydrogel, where the blue chains represent the polymer chains, and the red dashed lines represent the cross-linking interactions between them. These materials possess unique characteristics, such as high water content and mechanical stability, and can achieve high conductivities, which makes them appropriate materials for the next generation of aqueous batteries [61]. Furthermore, the use of semi-solid electrolytes allows manufacturing power sources with different shapes, which is an essential requirement for emerging technologies, but is not feasible for current rigid batteries [5, 62].
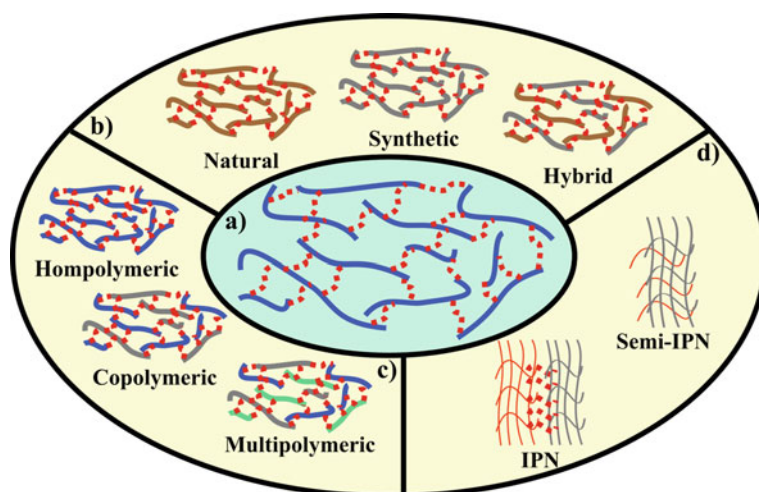

Fig. 9 Illustration of hydrogel microstructure and some of its classifications. **a** Basic microstructure of a hydrogel. **b** and **c** classification according to the origin of the polymer (or monomer) and the number of polymers used in the hydrogel synthesis, respectively. **d** Classification according to the interaction of different polymer matrixes

There are many ways to classify hydrogels according to their structure, polymer origin, and function [60, 61, 63, 64]. As to the origin of the polymers (or monomers) applied in the synthesis procedure, hydrogels can be natural-derived, synthetic, or hybrid, when a combination of natural and synthetic is used (Fig. 9b) [61, 63]. Examples of natural, synthetic, and hybrid hydrogels include gelatin [65], polyacrylic acid (PAA) [66], and carboxymethyl cellulose with polyethylene oxide networks [67]. Homopolymeric hydrogels are produced using only one polymer, copolymeric uses two different polymers, and multipolymeric uses three or more polymers, as shown in Fig. 9c [64]. Copolymeric hydrogels can be further classified into semi-interpenetrating (semi-IPN) and interpenetrating (IPN) networks. Semi-IPN occurs when some linear single chains of one polymer penetrate the porous structure of the cross-linked polymer. In contrast, IPN uses two polymeric cross-linked networks of different polymers that interact with each other by physical means [61, 63]. Figure 9d presents a sketch of the IPN and semi-IPN hydrogels. Both IPN and semi-IPN hydrogels have been employed as electrolytes in ESDs development [68, 69]. In terms of the charge content of the polymer backbone or pendant groups, hydrogels are classified as neutral, anionic, cationic, or ampholytic, when both cationic and anionic charges are present [61, 63, 64]. Finally, these materials can be classified according to their multifunctional properties, such as self-healing [70] and ionic conductivity [71].

The 3D hierarchical structure of hydrogels is built by physical or chemical means [72]. Physical hydrogels use physical interactions, such as electrostatic interactions [73], hydrogen bonding [73, 74], $\pi-\pi$ stacking [75], and hydrophobic interactions [74] as the driving force to achieve the gel state. Chemical hydrogels are synthesized by covalently bonding the polymer chains, which can be achieved by free-radical polymerization [76], the addition of a cross-linker agent [77], condensation reactions between organic functions [78], and click chemistry [79, 80]. Since covalent bonds are stronger than physical interactions, these hydrogels have improved mechanical properties [64]. However, the use of some cross-linkers [81, 82] enhances hydrogel toxicity, which is a concern in applications where biocompatibility is mandatory.

The next step in energy-storage technology is to develop new technologies thinking in the entire production chain, that is, from device manufacturing through to disposal or recycling [83]. Natural polymers are extracted from natural sources (e.g., alginate, chitosan, and agarose) and have key characteristics such as renewability, biocompatibility, biodegradability, and low cost [10]. Moreover, their aqueous solubility and wide range of organic functions make these polymers suitable for the construction of natural hydrogels which are also biocompatible and biodegradable [10, 59]. These characteristics make natural hydrogels appropriate materials for the next generation of ESDs, with a view to meeting the requirements of incipient technologies and addressing current environmental issues. The next section reviews recent advances in the application of natural-based hydrogels for the development of reliable and safe batteries.

3.1 Batteries Employing Natural-Based Hydrogels as Electrolyte

Researchers around the world have been searching for alternative materials to manufacture ESDs that meet the safety and flexibility requirements of wearable, ingestible, and implantable devices [4, 5, 84]. Since hydrogels possess high water content [85], and can achieve high ionic conductivities [86, 87], they can replace liquid aqueous electrolytes, which make the battery safer [88] and allow it to be produced in different shapes [65, 70], including flexible ones [11].

Crespilho et al. [89] obtained insights into the RFB research field and used previously reported molecules [36] incorporated in an easily synthesized agarose-based hydrogel to produce an organic/organometallic bioinspired secondary microbattery (MB). To produce the hydrogel electrolytes, bis(3-trimethylammonio) propyl viologen (BTMAP-Vi) and bis((3-thimethylammonio)propyl) ferrocene (BTMAP-Fc) were incorporated in 1.5% (w/w) agarose in 1 mol L^{-1} KCl solution and heated to 90 °C, after which the hot solutions were dripped onto flexible carbon fiber electrode surfaces. Gelation then occurred at room temperature [89].

The MB was assembled by placing a piece of previously hydrated Selemion® DSV membrane on the hydrogel/electrode surface, the union of cathodic and anodic chambers, and sealing with silicone resin. Figure 10a shows the assembled MB. To evaluate the maximum capacity of the MB, it was potentiostatically charged at 1.10 V until reaching an SOC of 92%, and then discharged at 0.30 V. The total discharged capacity was calculated as 0.79 mAh (Fig. 10b). At an SOC of 20%, the MB could supply 20 μA cm^{-2} for 100 h, which demonstrates a volumetric capacity of 0.021 mAh cm^{-2} μm^{-1}. Figure 10c shows the results of the galvanostatic charge–discharge cycling at 40 mA cm^{-2}. The charging and discharging capacities showed almost no change over 100 cycles, giving a CE ranging from 94 to 97%. In addition to its electrochemical characteristics, the MB exhibited attractive toxicological and structural characteristics. It is non-flammable, since it uses water as the solvent, and possesses low toxicity, because the quantities of BTMAP-Vi and BTMAP-Fc employed are low to cause harmful effects [89]. Thus, the electrochemical, structural, and toxicological characteristics make this battery suitable for low-power consumption medical devices, such as ingestible pills [90].

Chitosan (CS) and polyvinyl alcohol (PVA), both biodegradable polymers, were employed in the synthesis of an alkaline electrolyte for application in a zinc-electrolytic manganese dioxide (Zn-EMD) battery. First, CS and PVA solutions were mixed in a 1:0.2 wt% ratio (CP solution) and poured into a silicone mold. Next, the CP solution was dried at 37 °C for 1200 min. Finally, the dried hydrogels were soaked in KOH solutions at different concentrations and at different times. The best properties were achieved by the hydrogel soaked in 5 M KOH solution for 45 min, known as {5}CP (Fig. 10d), which achieved the highest swelling ratio, highest conductivity (457.19 mS cm^{-1}), and a lower degree of crystallinity. This hydrogel was then used as a gel polymer electrolyte in a Zn-EMD battery [91].
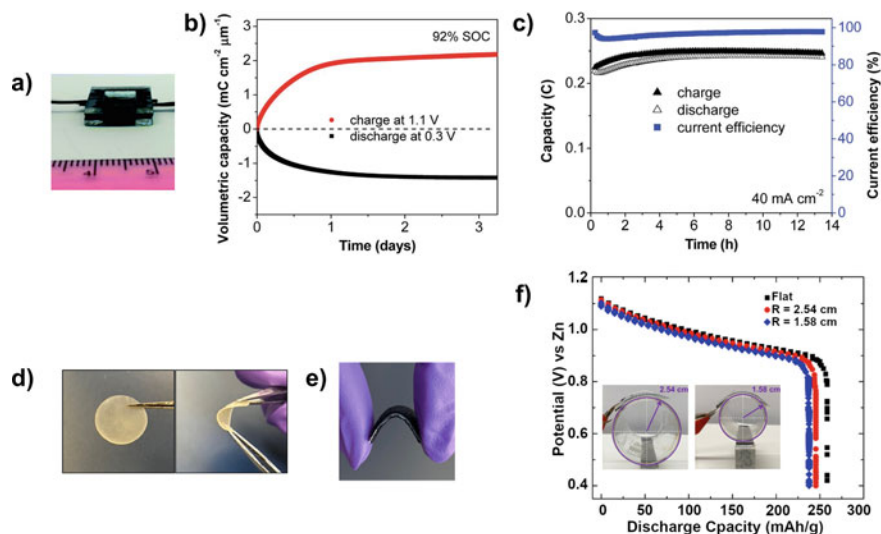
Fig. 10 Semi-solid batteries produced with polysaccharides. **a** Photograph, **b** potentiostatic charge–discharge curves at 1.10 (red) and 0.30 **V** (black), and **c** Charge and discharge capacities and CE over 100 cycles at 40 mA cm^{-2} for microbattery built up with BTMAP-Fc and BTMAP-Vi. **d** Photograph of CP samples, **e** photograph of Zn-EMD flexible battery, and **f** galvanostatic discharge for the Zn-EMD battery under two bent conditions. Reproduced from Ref. [89] with permission from Royal Society of Chemistry, Reprinted (adapted) with permission from Ref. [91]. Copyright 2021 American Chemical Society

Figure 10e shows the produced Zn-EMD battery. Pre-treated flexible carbon cloths (CC) were used as current collectors in both cathode and anode. The battery was assembled using a metallic zinc foil as the anode, CC coated with EMD ink as the cathode (load of ~1.4 mg cm^{-2}), and {5}CP as both electrolyte and separator. In order to achieve better cathode-electrolyte contact, {5}CP was previously dipped in CP solution until becoming gooey and then placed on the cathode surface [91]. The Zn-EMD battery was further characterized by galvanostatic charge–discharge at 0.1 A g^{-1} at two different potential windows, that is, 0.4–1.2 V (low potential) and 0.4–1.6 V (high potential), chosen according to the cathode degradation potential. The low and high potential windows presented a specific capacity of 310 and 287 mAh g^{-1} after the first cycle and capacity retention of 74% and 17.4% after 50 cycles, respectively. These results are attributed to EMD's irreversible phase transition to δ-MnO$_2$, which leads to an enhancement of the battery impedance and prevents charge transfer between the electrode and electrolyte. Furthermore, energy dispersive x-ray analysis shows a higher content of ZnMn$_x$O$_y$ complexes after further cycling at the higher voltage window, which also contributes to the inferior performance of the battery cycled at this potential window. The Zn-EMD battery was further galvanostatic cycled at 0.5 A g^{-1} and showed an average specific capacity of 175 mAh g^{-1} over 300 cycles with a CE of 96.5%. However, at this current density, the battery presented a steady decrease in capacity during the first 15 cycles. Finally,

to demonstrate the battery's flexibility, it was electrochemically characterized in two bent conformations and there was almost no change in the electrochemical performance, as shown in Fig. 10f [91].

Similarly, an alginate-based glycerol-plasticized hydrogel was developed and applied to zinc-iodide ($Zn-I_2$) batteries [71]. First, 0.75 g of glycerol was added to 50 mL of 30 mg mL^{-1} sodium alginate solution, with further stirring for 1 h. The resulting solution was cast on the cathode surface, degassed, and dried at 60 °C for 12 h. Finally, it was soaked in 1 mol L^{-1} zinc sulfate or acetate solution for 4 h. Figure 11a shows photographs of the alginate-based hydrogel. It could be bent or twisted without damage and even bear a weight of 200 g, which demonstrates its mechanical robustness and flexibility. The linear sweep voltammograms and electrochemical impedance spectroscopy measurements showed an operational voltage window of ~2.60 V and conductivity of 32.8 mS cm^{-1}, respectively. Finally, the hydrogel was capable of preventing zinc corrosion and I_2 shuttling, two mechanisms of $Zn-I_2$ battery failure; this affords a longer life for the novel batteries [71].

The semi-solid $Zn-I_2$ battery was assembled in a CR2025 shape with a zinc foil as the anode, the alginate-based hydrogel as the electrolyte, and a graphite paper coated with I_2@AC composite as the cathode. Galvanostatic charge–discharge at 0.2 A g^{-1} measurements with the $Zn(Ac)_2$-soaked alginate hydrogel showed a specific capacity, capacity retention, and CE of 183.4 mAh g^{-1} (Fig. 11b), 97.6%, and 99.3% over 200 cycles, respectively. For comparison, the authors also reported a $Zn-I_2$ battery with fiberglass soaked in $ZnSO_4$ as the separator. This battery exhibited a significantly inferior electrochemical performance (blue line in Fig. 9b). The galvanostatic charge–discharge assay at 1 A g^{-1} (Fig. 11c) shows capacity retention and CE of 66.8 and 99.5%, respectively, which demonstrates the long life of the battery and the shielding effects of the hydrogel over the zinc anode. Finally, a flexible pouch battery was assembled using this approach. This battery shows an OCV of 1.25 V, capacity of 3.0–3.5 mAh, and worked properly even in bent conformations [71].

Self-healing hydrogels can repair themselves after damage and have been suggested as an alternative to enhance the lifespan of batteries. In this context, a copolymeric hydrogel based on alginate and PAA was synthesized and applied as an electrolyte to build an aqueous lithium-ion yarn battery (ALIYB). To synthesize the hydrogel, PANa-Ca-SA, a solution of acrylic acid and bistrimethanesulfonimide lithium salt was neutralized with NaOH in an ice bath. Then, alginate, calcium chloride, and ammonium persulfate were dissolved in the solution and the resulting solution was kept at 40 °C for 30 h to allow polymerization. Calcium ions play a key role in this hydrogel as they electrostatically interact with PAA and alginate polymers and act as cross-linkers of the two polymeric networks. In addition, the electrostatic interaction between calcium ions and the polymers explains the remarkable self-healing property of the hydrogel, because it can easily be broken and healed (Fig. 11d). The authors investigated the influence of the cutting/self-healing cycles on the electrical and mechanical properties of the hydrogel. The results showed a small decrease in the PANa-Ca-SA conductivity, which was 88% of its initial value after the eighth cutting/self-healing cycle. In contrast, the mechanical properties showed a pronounced change. The original hydrogel could be stretched at 350% strain and
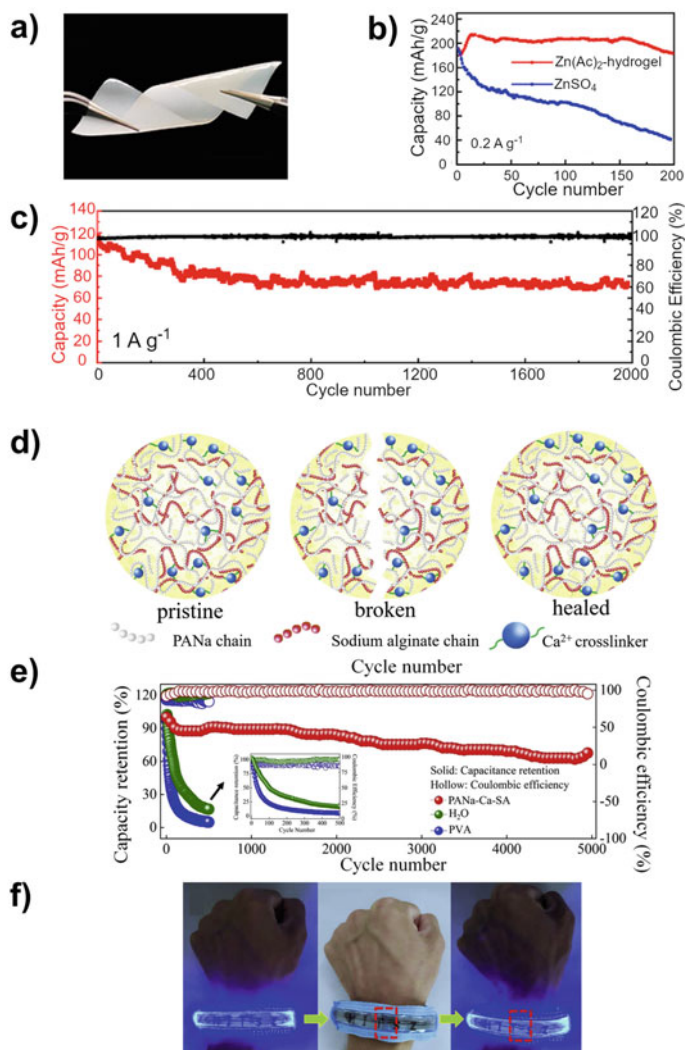
Fig. 11 Batteries produced using hybrid alginate-based hydrogel as electrolyte. **a** Photograph of twisted alginate-based hydrogel electrolyte, **b** discharge capacity at 0.2 A g^{-1} for Zn/I$_2$ batteries using the alginate-based hydrogel (red line) and aqueous Zn(Ac)$_2$ solution as electrolytes, respectively. **c** Capacity (red line) and CE (black line) for Zn/I$_2$ battery assembled with alginate-based electrolyte under galvanostatic cycling at 1 A g^{-1} over 2000 cycles. **d** Representation of pristine, broken and healed PANa-Ca-SA hydrogel. **e** Electrochemical performances of ALIYBs produced using PANa-Ca-SA hydrogel (red), water (green) and, PVA-based hydrogel (blue) electrolytes over 5000 cycles. **f** Photograph of a light strip powered by four ALIYBs before cutting (left), after cut (middle), and after self-healing (right). Reprinted (adapted) with permission from Ref. [71]. Copyright 2021 American Chemical Society. Reprinted from Energy-storage materials, v.28, Ji, Z et al., A both microscopically and macroscopically intrinsic self-healing long lifespan yarn battery, p. 334–341, Copyright (2021), with permission from Elsevier

235 kPa tensile strength, while for the eight-cut hydrogel these values were reduced to 48% and 45 kPa [70].

The ALIYB was assembled using PANa-Ca-SA as the electrolyte and $LiMn_2O_4$ and LiV_3O_8 coated yarns as the anode and cathode, respectively. The galvanostatic charge–discharge data at 0.5 A g^{-1} (Fig. 11e) show capacity retention and CE of 70% and nearly 100% after 5000 cycles, respectively. This behavior is much better than that of water and PVA-hydrogel-based lithium-ion batteries and is attributed to the self-healing capacity of the hydrogel, which prevents damage to the surfaces of the electrodes caused by the insertion and extraction of lithium ions. Furthermore, the ALIYB showed a healing efficiency of 68% and almost no change in its electrochemical performance after eight cutting/self-healing cycles. Figure 11f shows the application of four parallel coupled batteries to power a light strip and evidence the self-healing behavior of the battery, because the device turns off when the battery breaks and shines again after the battery has healed [70].

4 Final Considerations

Electrochemical ESDs are indispensable for the ongoing sustainable development of humankind because they are highly efficient and address the current environmental concerns. Moreover, nature-developed pathways and materials have inspired researchers to confront the global problems that arise from the high consumption of non-renewable energy sources. In the energy-research field, organic-based RFBs that use quinones and flavins; and flexible batteries that use natural-based gel electrolytes, are key examples of this integration. However, both technologies are in their infancy and their advancement will require a multidisciplinary effort in areas such as materials science, chemical synthesis and electrosynthesis, electrochemistry, polymer science, soft materials, quantum chemistry, and engineering, among others.

References

1. Yang, Z., Zhang, J., Kintner-Meyer, M.C.W., et al.: Electrochemical energy storage for green grid. Chem. Rev. **111**, 3577–3613 (2011). https://doi.org/10.1021/cr100290v
2. Nguyen, T., Savinell, R.F.: Flow batteries. Electrochem. Soc. Interface **19**, 54–56 (2010). https://doi.org/10.1149/2.F06103if
3. Koydemir, H.C., Ozcan, A.: Wearable and implantable sensors for biomedical applications. Annu. Rev. Anal. Chem. **11**, 127–146 (2018). https://doi.org/10.1146/annurev-anchem-061417-125956

4. Ling, Y., An, T., Yap, L.W., et al.: Disruptive, soft, wearable sensors. Adv. Mater. **32**, 1904664 (2020). https://doi.org/10.1002/adma.201904664

5. Sunwoo, S.-H., Ha, K.-H., Lee, S., et al.: Wearable and implantable soft bioelectronics: device designs and material strategies. Annu. Rev. Chem. Biomol. Eng. **12**, 359–391 (2021). https://doi.org/10.1146/annurev-chembioeng-101420-024336

6. Whitesides, G.M., Whitesides, G.M.: Bioinspiration: something for everyone (2015)

7. Monks, T.J., Hanzlik, R.P., Cohen, G.M., et al.: Quinone chemistry and toxicity. Toxicol. Appl. Pharmacol. **112**, 2–16 (1992). https://doi.org/10.1016/0041-008X(92)90273-U

8. Son, E.J., Kim, J.H., Kim, K., Park, C.B.: Quinone and its derivatives for energy harvesting and storage materials. J. Mater. Chem. A **4**, 11179–11202 (2016). https://doi.org/10.1039/C6TA03123D

9. Massey, V.: The chemical and biological versatility of riboflavin. Biochem. Soc. Trans. **28**, 283–296 (2000). https://doi.org/10.1042/bst0280283

10. Cui, C., Fu, Q., Meng, L., et al.: Recent progress in natural biopolymers conductive hydrogels for flexible wearable sensors and energy devices: materials, structures, and performance. ACS Appl. Bio. Mater. **4**, 85–121 (2021). https://doi.org/10.1021/acsabm.0c00807

11. Cheng, X., Pan, J., Zhao, Y., et al.: Gel polymer electrolytes for electrochemical energy storage. Adv. Energy Mater. **8**, 1–16 (2018). https://doi.org/10.1002/aenm.201702184

12. Prifti, H., Parasuraman, A., Winardi, S., et al.: Membranes for redox flow battery applications. Membranes (Basel) **2**, 275–306 (2012). https://doi.org/10.3390/membranes2020275

13. Winsberg, J., Hagemann, T., Janoschka, T., et al.: Redox-flow batteries: from metals to organic redox-active materials. Angew. Chemie Int. Ed. **56**, 686–711 (2017). https://doi.org/10.1002/anie.201604925

14. Leung, P., Shah, A.A., Sanz, L., et al.: Recent developments in organic redox flow batteries: a critical review. J. Power Sour. **360**, 243–283 (2017). https://doi.org/10.1016/j.jpowsour.2017.05.057

15. Sánchez-Díez, E., Ventosa, E., Guarnieri, M., et al.: Redox flow batteries: status and perspective towards sustainable stationary energy storage. J. Power Sour. **481**, 228804 (2021). https://doi.org/10.1016/j.jpowsour.2020.228804

16. Alotto, P., Guarnieri, M., Moro, F.: Redox flow batteries for the storage of renewable energy: a review. Renew. Sustain. Energy Rev. **29**, 325–335 (2014). https://doi.org/10.1016/j.rser.2013.08.001

17. Kazacos, M., Cheng, M., Skyllas-Kazacos, M.: Vanadium redox cell electrolyte optimization studies. J. Appl. Electrochem. **20**, 463–467 (1990). https://doi.org/10.1007/BF01076057

18. Rahman, F., Skyllas-Kazacos, M.: Vanadium redox battery: positive half-cell electrolyte studies. J. Power Sour. **189**, 1212–1219 (2009). https://doi.org/10.1016/j.jpowsour.2008.12.113

19. Rahman, F., Skyllas-Kazacos, M.: Solubility of vanadyl sulfate in concentrated sulfuric acid solutions. J. Power Sour. **72**, 105–110 (1998). https://doi.org/10.1016/S0378-7753(97)02692-X

20. Huskinson, B., Marshak, M.P., Suh, C., et al.: A metal-free organic–inorganic aqueous flow battery. Nature **505**, 195–198 (2014). https://doi.org/10.1038/nature12909

21. Gerhardt, M.R., Tong, L., Gómez-Bombarelli, R., et al.: Anthraquinone derivatives in aqueous flow batteries. Adv. Energy Mater. **7**, 1601488 (2017). https://doi.org/10.1002/aenm.201601488

22. Yang, Z., Tong, L., Tabor, D.P., et al.: Alkaline benzoquinone aqueous flow battery for large-scale storage of electrical energy. Adv. Energy Mater. **8**, 1702056 (2018). https://doi.org/10.1002/aenm.201702056

23. Lin, K., Chen, Q., Gerhardt, M.R., et al.: Alkaline quinone flow battery. Science **349**(80), 1529–1532 (2015). https://doi.org/10.1126/science.aab3033

24. Er, S., Suh, C., Marshak, M.P., Aspuru-Guzik, A.: Computational design of molecules for an all-quinone redox flow battery. Chem. Sci. **6**, 885–893 (2015). https://doi.org/10.1039/C4SC03030C

25. Bachman, J.E., Curtiss, L.A., Assary, R.S.: Investigation of the redox chemistry of anthraquinone derivatives using density functional theory. J. Phys. Chem. A **118**, 8852–8860 (2014). https://doi.org/10.1021/jp5060777

26. Lee, W., Park, G., Kwon, Y.: Alkaline aqueous organic redox flow batteries of high energy and power densities using mixed naphthoquinone derivatives. Chem. Eng. J. **386**, 123985 (2020). https://doi.org/10.1016/j.cej.2019.123985

27. Yang, B., Hoober-Burkhardt, L., Wang, F., et al.: An inexpensive aqueous flow battery for large-scale electrical energy storage based on water-soluble organic redox couples. J. Electrochem. Soc. **161**, A1371–A1380 (2014). https://doi.org/10.1149/2.1001409jes

28. Lima, A. R.F., Pereira, R.C., Azevedo, J., et al.: On the path to aqueous organic redox flow batteries: Alizarin red S alkaline negolyte. Performance evaluation and photochemical studies. J. Mol. Liq. **336**, 116364 (2021). https://doi.org/10.1016/j.molliq.2021.116364

29. Zhou, M., Chen, Y., Salla, M., et al.: Single-molecule redox-targeting reactions for a pH-neutral aqueous organic redox flow battery. Angew. Chem. Int. Ed. **59**, 14286–14291 (2020). https://doi.org/10.1002/anie.202004603

30. Lee, W., Permatasari, A., Kwon, B.W., Kwon, Y.: Performance evaluation of aqueous organic redox flow battery using anthraquinone-2,7-disulfonic acid disodium salt and potassium iodide redox couple. Chem. Eng. J. **358**, 1438–1445 (2019). https://doi.org/10.1016/j.cej.2018.10.159

31. Guiheneuf, S., Lê, A., Godet-Bar, T., et al.: Behaviour of 3,4-dihydroxy-9,10-anthraquinone-2-sulfonic acid in alkaline medium: towards a long-cycling aqueous organic redox flow battery. ChemElectroChem **8**, 2526–2533 (2021). https://doi.org/10.1002/celc.202100284

32. Hu, B., Luo, J., Hu, M., et al.: A pH-neutral, metal-free aqueous organic redox flow battery employing an ammonium anthraquinone anolyte. Angew. Chem. **131**, 16782–16789 (2019). https://doi.org/10.1002/ange.201907934

33. Lai, Y.Y., Li, X., Liu, K., et al.: Stable low-cost organic dye anolyte for aqueous organic redox flow battery. ACS Appl. Energy Mater. **3**, 2290–2295 (2020). https://doi.org/10.1021/acsaem.9b01735

34. Liu, T., Wei, X., Nie, Z., et al.: A total organic aqueous redox flow battery employing a low cost and sustainable methyl viologen anolyte and 4-HO-TEMPO catholyte. Adv. Energy Mater. **6**, 1501449 (2016). https://doi.org/10.1002/aenm.201501449

35. Liu, L., Yao, Y., Wang, Z., Lu, Y.-C.: Viologen radical stabilization by molecular spectators for aqueous organic redox flow batteries. Nano Energy **84**, 105897 (2021). https://doi.org/10.1016/j.nanoen.2021.105897

36. Beh, E.S., De Porcellinis, D., Gracia, R.L., et al.: A neutral pH aqueous organic-organometallic redox flow battery with extremely high capacity retention. ACS Energy Lett. **2**, 639–644 (2017). https://doi.org/10.1021/acsenergylett.7b00019

37. Hu, B., DeBruler, C., Rhodes, Z., Liu, T.L.: Long-cycling aqueous organic redox flow battery (AORFB) toward sustainable and safe energy storage. J. Am. Chem. Soc. **139**, 1207–1214 (2017). https://doi.org/10.1021/jacs.6b10984

38. Tsehaye, M.T., Yang, X., Janoschka, T., et al.: Study of anion exchange membrane properties incorporating N-spirocyclic quaternary ammonium cations and aqueous organic redox flow battery performance. Membranes **11** (2021)

39. Xing, X., Huo, Y., Wang, X., et al.: A benzophenone-based anolyte for high energy density all-organic redox flow battery. Int. J. Hydrog. Energy **42**, 17488–17494 (2017)

40. Sreenath, S., Nayanthara, P.S., Pawar, C.M., et al.: Phenolic triamine dangling poly(VDF-co-HFP) anion exchange membrane for all aqueous organic redox flow battery. J. Energy Storage **40**, 102689 (2021). https://doi.org/10.1016/j.est.2021.102689

41. Lin, K., Gómez-Bombarelli, R., Beh, E.S., et al.: A redox-flow battery with an alloxazine-based organic electrolyte. Nat. Energy **1**, 1–8 (2016). https://doi.org/10.1038/nenergy.2016.102

42. Orita, A., Verde, M.G., Sakai, M., Meng, Y.S.: A biomimetic redox flow battery based on flavin mononucleotide. Nat. Commun. **7**, 1–8 (2016). https://doi.org/10.1038/ncomms13230

43. Quan, M., Sanchez, D., Wasylkiw, M.F., Smith, D.K.: Voltammetry of quinones in unbuffered aqueous solution: reassessing the roles of proton transfer and hydrogen bonding in the aqueous electrochemistry of quinones. J. Am. Chem. Soc. **129**, 12847–12856 (2007). https://doi.org/10.1021/ja0743083

44. Kim, K.C., Liu, T., Lee, S.W., Jang, S.S.: First-principles density functional theory modeling of li binding: thermodynamics and redox properties of quinone derivatives for lithium-ion batteries. J. Am. Chem. Soc. **138**, 2374–2382 (2016). https://doi.org/10.1021/jacs.5b13279

45. Xu, Y., Wen, Y., Cheng, J., et al.: Study on a single flow acid Cd-chloranil battery. Electrochem. Commun. **11**, 1422–1424 (2009). https://doi.org/10.1016/j.elecom.2009.05.021
46. Xu, Y., Wen, Y.-H., Cheng, J., et al.: A study of tiron in aqueous solutions for redox flow battery application. Electrochim. Acta **55**, 715–720 (2010). https://doi.org/10.1016/j.electacta.2009.09.031
47. Hofmann, J.D., Schröder, D.: Which parameter is governing for aqueous redox flow batteries with organic active material? Chem. Ing. Tech. **91**, 786–794 (2019). https://doi.org/10.1002/cite.201800162
48. Yang, B., Hoober-Burkhardt, L., Krishnamoorthy, S., et al.: High-performance aqueous organic flow battery with quinone-based redox couples at both electrodes. J. Electrochem. Soc. **163**, A1442–A1449 (2016). https://doi.org/10.1149/2.1371607jes
49. Wu, M., Jing, Y., Wong, A.A., et al.: Extremely stable anthraquinone negolytes synthesized from common precursors. Chemistry **6**, 1432–1442 (2020). https://doi.org/10.1016/j.chempr.2020.03.021
50. Jing, Y., Wu, M., Wong, A.A., et al.: In situ electrosynthesis of anthraquinone electrolytes in aqueous flow batteries. Green Chem. **22**, 6084–6092 (2020). https://doi.org/10.1039/D0GC02236E
51. Sedenho, G.C., De Porcellinis, D., Jing, Y., et al.: Effect of molecular structure of quinones and carbon electrode surfaces on the interfacial electron transfer process. ACS Appl. Energy Mater. **3**, 1933–1943 (2020). https://doi.org/10.1021/acsaem.9b02357
52. Miura, R.: Versatility and specificity in flavoenzymes: control mechanisms of flavin reactivity. Chem. Rec. **1**, 183–194 (2001). https://doi.org/10.1002/tcr.1007
53. Entsch, B., Ballou, D.P.: Flavins. In: Encyclopedia of Biological Chemistry, pp. 309–313. Elsevier (2013)
54. Fagan, R.L., Palfey, B.A.: Flavin-dependent enzymes. In: Comprehensive Natural Products II, pp. 37–113. Elsevier (2010)
55. Kalantar-Zadeh, K., Ha, N., Ou, J.Z., Berean, K.J.: Ingestible sensors. ACS Sens. **2**, 468–483 (2017). https://doi.org/10.1021/acssensors.7b00045
56. Samad, L., Ali, M., Ramzi, H.: Button battery ingestion: Hazards of esophageal impaction. J. Pediatr. Surg. **34**, 1527–1531 (1999). https://doi.org/10.1016/S0022-3468(99)90119-7
57. Chevin, J.C., Attik, G., Dika, H., et al.: Button battery induced cell damage: a pathophysiological study. Electrochem. Commun. **10**, 1756–1760 (2008). https://doi.org/10.1016/j.elecom.2008.09.002
58. Mankowski, P.J., Kanevsky, J., Bakirtzian, P., Cugno, S.: Cellular phone collateral damage: a review of burns associated with lithium battery powered mobile devices. Burns **42**, e61–e64 (2016). https://doi.org/10.1016/j.burns.2015.10.012
59. Catoira, M.C., Fusaro, L., Di Francesco, D., et al.: Overview of natural hydrogels for regenerative medicine applications. J. Mater. Sci. Mater. Med. **30**, 115 (2019). https://doi.org/10.1007/s10856-019-6318-7
60. Guo, Y., Bae, J., Zhao, F., Yu, G.: Functional hydrogels for next-generation batteries and supercapacitors. Trends Chem. **1**, 335–348 (2019). https://doi.org/10.1016/j.trechm.2019.03.005
61. Guo, Y., Bae, J., Fang, Z., et al.: Hydrogels and hydrogel-derived materials for energy and water sustainability. Chem. Rev. **120**, 7642–7707 (2020). https://doi.org/10.1021/acs.chemrev.0c00345
62. Yang, Z., Deng, J., Chen, X., et al.: A highly stretchable, fiber-shaped supercapacitor. Angew. Chem. Int. Ed. **52**, 13453–13457 (2013). https://doi.org/10.1002/anie.201307619
63. Thakur, V.K., Thakur, M.K.: Hydrogels: Recent Advances. Springer, Sinpagore (2018)
64. Ali, A., Ahmed, S.: Recent advances in edible polymer based hydrogels as a sustainable alternative to conventional polymers. J. Agric. Food Chem. **66**, 6940–6967 (2018). https://doi.org/10.1021/acs.jafc.8b01052
65. Park, J., Park, M., Nam, G., et al.: All-solid-state cable-type flexible zinc-air battery. Adv. Mater. **27**, 1396–1401 (2015). https://doi.org/10.1002/adma.201404639

66. Tran, T.N.T., Chung, H.-J., Ivey, D.G.: A study of alkaline gel polymer electrolytes for rechargeable zinc—Air batteries. Electrochim Acta **327**, 135021 (2019). https://doi.org/10.1016/j.electacta.2019.135021

67. Colò, F., Bella, F., Nair, J.R., et al.: Cellulose-based novel hybrid polymer electrolytes for green and efficient Na-ion batteries. Electrochim Acta **174**, 185–190 (2015). https://doi.org/10.1016/j.electacta.2015.05.178

68. Wang, P.-H., Tseng, L.-H., Li, W.-C., et al.: Zwitterionic semi-IPN electrolyte with high ionic conductivity and high modulus achieving flexible 2.4 V aqueous supercapacitors. J. Taiwan Inst. Chem. Eng. **126**, 58–66 (2021). https://doi.org/10.1016/j.jtice.2021.06.044

69. Yan, T., Zou, Y., Zhang, X., et al.: Hydrogen bond interpenetrated agarose/PVA network: a highly ionic conductive and flame-retardant gel polymer electrolyte. ACS Appl. Mater. Interfaces **13**, 9856–9864 (2021). https://doi.org/10.1021/acsami.0c20702

70. Ji, Z., Wang, H., Chen, Z., et al.: A both microscopically and macroscopically intrinsic self-healing long lifespan yarn battery. Energy Storage Mater. **28**, 334–341 (2020). https://doi.org/10.1016/j.ensm.2020.03.020

71. Shang, W., Zhu, J., Liu, Y., et al.: Establishing high-performance quasi-solid Zn/I_2 batteries with alginate-based hydrogel electrolytes. ACS Appl. Mater. Interfaces **13**, 24756–24764 (2021). https://doi.org/10.1021/acsami.1c03804

72. Varaprasad, K., Raghavendra, G.M., Jayaramudu, T., et al.: A mini review on hydrogels classification and recent developments in miscellaneous applications. Mater. Sci. Eng. C **79**, 958–971 (2017). https://doi.org/10.1016/j.msec.2017.05.096

73. Lin, Y., Zhang, H., Liao, H., et al.: A physically crosslinked, self-healing hydrogel electrolyte for nano-wire PANI flexible supercapacitors. Chem. Eng. J. **367**, 139–148 (2019). https://doi.org/10.1016/j.cej.2019.02.064

74. Xu, R., Ma, S., Lin, P., et al.: High strength astringent hydrogels using protein as the building block for physically cross-linked multi-network. ACS Appl. Mater. Interfaces **10**, 7593–7601 (2018). https://doi.org/10.1021/acsami.7b04290

75. Wang, H., Zhou, C., Zhu, H., et al.: Hierarchical porous carbons from carboxylated coal-tar pitch functional poly(acrylic acid) hydrogel networks for supercapacitor electrodes. RSC Adv. **10**, 1095–1103 (2020). https://doi.org/10.1039/C9RA09141F

76. Wang, Z., Mo, F., Ma, L., et al.: Highly compressible cross-linked polyacrylamide hydrogel-enabled compressible $Zn–MnO_2$ battery and a flexible battery-sensor system. ACS Appl. Mater. Interfaces **10**, 44527–44534 (2018). https://doi.org/10.1021/acsami.8b17607

77. Zerbinati, N., Esposito, C., Cipolla, G., et al.: Chemical and mechanical characterization of hyaluronic acid hydrogel cross-linked with polyethylen glycol and its use in dermatology. Dermatol. Ther. **33**, e13747 (2020). https://doi.org/10.1111/dth.13747

78. Koo, B., Kim, H., Cho, Y., et al.: A highly cross-linked polymeric binder for high-performance silicon negative electrodes in lithium ion batteries. Angew. Chem. Int. Ed. **51**, 8762–8767 (2012). https://doi.org/10.1002/anie.201201568

79. Li, Y., Wang, X., Han, Y., et al.: Click chemistry-based biopolymeric hydrogels for regenerative medicine. Biomed. Mater. **16** (2021). https://doi.org/10.1088/1748-605X/abc0b3

80. Zhang, Y., Liu, S., Li, T., et al.: Cytocompatible and non-fouling zwitterionic hyaluronic acid-based hydrogels using thiol-ene "click" chemistry for cell encapsulation. Carbohydr. Polym. **236**, 116021 (2020). https://doi.org/10.1016/j.carbpol.2020.116021

81. Liu, K., Wei, S., Song, L., et al.: Conductive hydrogels—A novel material: recent advances and future perspectives. J. Agric. Food Chem. **68**, 7269–7280 (2020). https://doi.org/10.1021/acs.jafc.0c00642

82. Ballantyne, B., Myers, R.C.: The acute toxicity and primary irritancy of glutaraldehyde solutions. Vet. Hum. Toxicol. **43**, 193–202 (2001)

83. Lithium-ion batteries need to be greener and more ethical. Nature **595**, 7 (2021). https://doi.org/10.1038/d41586-021-01735-z

84. Liu, X., Steiger, C., Lin, S., et al.: Ingestible hydrogel device. Nat. Commun. **10**, 493 (2019). https://doi.org/10.1038/s41467-019-08355-2

85. Qian, C., Higashigaki, T., Asoh, T.-A., Uyama, H.: Anisotropic conductive hydrogels with high water content. ACS Appl. Mater. Interfaces **12**, 27518–27525 (2020). https://doi.org/10.1021/acsami.0c06853

86. Wang, Y., Zhang, L., Lu, A.: Transparent, antifreezing, ionic conductive cellulose hydrogel with stable sensitivity at subzero temperature. ACS Appl. Mater. Interfaces **11**, 41710–41716 (2019). https://doi.org/10.1021/acsami.9b15849

87. Liang, Y., Ye, L., Sun, X., et al.: Tough and stretchable dual ionically cross-linked hydrogel with high conductivity and fast recovery property for high-performance flexible sensors. ACS Appl. Mater. Interfaces **12**, 1577–1587 (2020). https://doi.org/10.1021/acsami.9b18796

88. Cui, Y., Chai, J., Du, H., et al.: Facile and reliable in situ polymerization of poly(Ethyl Cyanoacrylate)-based polymer electrolytes toward flexible lithium batteries. ACS Appl. Mater. Interfaces **9**, 8737–8741 (2017). https://doi.org/10.1021/acsami.6b16218

89. Crespilho, F.N., Sedenho, G.C., De Porcellinis, D., et al.: Non-corrosive, low-toxicity gel-based microbattery from organic and organometallic molecules. J. Mater. Chem. A (2019). https://doi.org/10.1039/C9TA08685D

90. Mark, M., Phillip, N., Alison, H., et al.: An ingestible bacterial-electronic system to monitor gastrointestinal health. Science **360**(80), 915–918 (2018). https://doi.org/10.1126/science.aas9315

91. Poosapati, A., Vadnala, S., Negrete, K., et al.: Rechargeable zinc-electrolytic manganese dioxide (EMD) battery with a flexible chitosan-alkaline electrolyte. ACS Appl. Energy Mater. **4**, 4248–4258 (2021). https://doi.org/10.1021/acsaem.1c00675